Materials Research Express

# Mechanical behavior associated with metallurgical aspects of friction stir welded Al-Li alloy exposed to exfoliation corrosion test

1
2
3
4
5
6
7
8
9
10
11
12
13
14
15
16
17
18
19
20
21
22
23
24
25
26
27
28
29
30
31
32
33
34
35
36
37
38
39
40
41
42
43
44
45
46
47
48
49
50
51
52
53
54
55
56
57
58
59
60

# Mechanical Behavior Associated with Metallurgical Aspects of Friction Stir Welded Al-Li Alloy Exposed to Exfoliation Corrosion Test

Hu Baiyao[1][*], Zhang Hua[2] and Khoshnaw Fuad[3]

[1]*School of Materials Science and Engineering, Tongji University, Shanghai 201804, China*

[2]*School of Mechanical Engineering, Beijing Institute of Petrochemical Technology, Beijing 102617, China*

[3]*School of Engineering and Sustainable Development, De Montfort University, Leicester LE1 9BH, United Kingdom*

## Abstract

This research aims to investigate the effect of the exfoliation corrosion exposure time on the mechanical properties, the strength and elongation, of friction stir welded Al-Li alloy type 2195-T8. The exfoliation corrosion test was performed using the exfoliation corrosion (EXCO) solution, based on ASTM G34. The samples were exposed to different exposure times 24, 48, 96, 192 and 384 hours. The results showed that both the strength and elongation of the welded specimens - exposed to the exfoliation corrosion tests - were reduced. For example, the samples that were exposed to 384 hrs, their initial tensile strength and elongation were reduced by 13% and 17% respectively. The degradation process due to the exfoliation corrosion on the tensile strength was divided into three stages: fast (0-96 hrs: 443.7 MPa-416.3 MPa, the degraded rate was 0.29 MPa/h), steady (96-192 hrs: 416.3 MPa-413.4 MPa, the degraded rate was 0.03 MPa/h) and medium rate (192-384 hrs: 413.4 MPa-386.7 MPa, the degraded rate was 0.14 MPa/h). For the elongation, in general, the reduction was similar to the style of strength, but with different rates. The TEM images showed that this degradation was due to the dissolution of $T_1$ (Al$_2$CuLi) and S´ (Al$_2$CuMg) phase. Also, the corrosion products and their role of adherence on the surface of the tested specimens were investigated. An empirical equation *p*-t (mechanical properties-exposure time) was established to calculate the effect of exposure corrosion time on the performance of welded specimens.

**Keyword**: Al-Li alloy 2195-T8; friction stir welding; exfoliation corrosion; ultimate tensile strength; elongation; empirical equation *p*-t

## 1. Introduction

In the last two decades, the Al-Li alloys have become widely used due to their good properties, reducing the weight structure by 10%-15% and increasing the stiffness to 15%-20% compared with traditional Al alloys, thereby becoming a candidate with great promise to replace other Al alloys [1-5]. Joining of aluminum alloys is a major process in many engineering applications, for example in aerospace. However, welding in general, and the fusion welding-based processes in particular, to some extends will limit the performance of Al-Li alloys, as it causes defects such as hot cracks, porosity, softening, difficultly removed oxide film, etc.

The friction stir welding FSW process noticeably reduces the defects that associate with the fusion welding-based methods. FSW is a solid-state, autogenously process without melting [6-8] and is extensively applied in joining Al-Li alloys [9,10]. In general, the welded parts by using FSW method are divided into a base material (BM), heat affected zone (HAZ), thermal-mechanical affect zone (TMAZ) and weld nugget zone (WNZ) [10], thus each zone shows different microstructure [11-13]. The precipitates in the BM primarily consist of $T_1$ ($Al_2CuLi$) and $\theta'$ ($Al_2Cu$) phases [11, 14, 15], while in HAZ the phases are $\delta'$ ($Al_3Li$) [14, 16-19], while there are reports show $S'$ ($Al_2CuMg$) phase in HAZ [10, 20-22]. In terms of WNZ, which is affected by both thermomechanical and stirring, both $\delta'$ and $\beta'$ ($Al_3Zr$) are the major strengthening phases [14, 16, 23, 24]. Due to these microstructural changes, many researchers have studied the corrosion performance of welded alloys [25-28]. Liu *et al.* [22] found that the high proportion of $T_1$ phase reduced the corrosion sensitivity of the 2198 Al-Li alloy. Ma *et al.* [29] reported that the dissolution of $T_1$ phase in FSW joint made the corrosion degree lower than BM in 2099 Al-Li alloy. Others [20, 30] found that the corrosion potential of $\theta'$ phase was higher than the matrix and was often acted as a cathode to promote the corrosion. Ren *et al.* [20] revealed two corrosion mechanisms of $S'$ phase, they found that pitting occurs around the $S'$ phase. Bousquet *et al.* [21] found out that HAZ was more sensitive to intergranular corrosion than the BM and other welding areas due to S/S′ phase precipitation along HAZ grain boundaries in welded alloys. Yi *et al.* [31] showed that the effect of $\delta'$ and $\beta'$ phase on local corrosion was relatively small, while the uniform corrosion was the main phenomenon. The microstructural characterization and mechanical properties of Al-Li alloy with FSW joints were studied by many researchers [32-34], however, the major concerns remained was about the corrosion behavior of the alloy. Li *et al.* [35] and Huang *et al.* [36] studied the

intergranular corrosion behaviors of 2195 Al-Li alloy and found that the intergranular corrosion of the alloy was related to $T_1$ phase. Luo *et al.* [37] and Li *et al.* [38] studied the corrosion behaviors of Al-Li alloys in sodium chloride solution, they found that general corrosion and localized corrosion of intergranular and pitting corrosion in the alloy.

There are some researchers have studied the influence of corrosive environment on the properties of aluminum alloys. Qiu *et al.* [39] studied the effect of corrosion on the mechanical parameters of aluminum alloy type 2024-T4, using ASTM G34 [40]. The results showed that the tensile strength and fatigue life are exponentially related to the average value of the corrosion rate. Liao *et al.* [41] found slightly different results using the fitting equation. Wang [42] indicated that the performance of 7075 alloys declined rapidly after the first two cycles (one cycle was 48h) against the marine atmospheric corrosion, while the decline rate of performance was relatively gentle with the extension of the test time. Khoshnaw [43] found that the exfoliation corrosion degree for 2024-T3 increased with increasing the aging time while decreased for 7075-T6. The results were attributed to the type of precipitants in both alloys. Ma *et al.* [44] demonstrated that the pre-corrosion damage and saline environment had significant effects on the detailed fatigue performance of 7xxx series aluminum alloy, which was consistent with the research of Lu *et al.* [45]. Su [46] compared the corrosion behavior and mechanical properties of 2D12 aluminum alloy and 5A90 Al-Li alloy by using marine environmental exposure. The results showed that the corrosion process of the 5A90 Al-Li alloy did not follow the law of power function, and the mechanical damage caused by corrosion was significantly greater than that of 2D12 alloy.

Since the mechanical and corrosion properties of alloys strongly depend on the microstructure, the type, size and distribution of the precipitates. Therefore, further studies on the precipitated phases will help to explain the influence of corrosion on the microstructure of Al-Li alloys. The phases, such as $T_1$, as the main strengthening phase of Al-Li alloy, might strongly affect the corrosion performance of the alloy. Li *et al.* [35] and Huang *et al.* [36], both showed that $T_1$ was closely related to the generation of intergranular corrosion, and Su *et al.* [46] confirmed the same outcomes. Luo *et al.* [37] found that discontinuous localized corrosion in Al-Li alloy is associated with corroded $\theta'$ ($Al_2Cu$) particles, as well as pits that are formed by particle fall-out due to dissolution of surrounding Al substrate. The exfoliation corrosion leads to the delamination of thin

metal layers, thus the strength and ductility of the welded alloys would be affected, consequently posed a serious threat to the safety of the structural parts [40].

Although there are studies have investigated the effect of corrosion, in general, on different Al alloys. There are still gaps in the effect of specific types of corrosion individually on the mechanical properties of welded Al-Li alloys. Therefore, this research aims to investigate the influence of the exfoliation corrosion on the mechanical properties of friction stir welded Al-Li alloy type 2195-T8.

## 2. Materials and Experimental Works

Plates, 8 mm thick, of Al-Li alloys type 2195-T8, were used in this study. The chemical composition analysis of the alloy was provided by Southwest Aluminum Corporation (Group) Co., Ltd. Table 1 shows the chemical composition of the alloy. The plates were cut into 100×650 mm, and every two pieces of the cut plates were welded by a numerical control Gantry type friction stir welding machine. The rotation speed and the welding speed were 800 rpm and 50 mm/min respectively.

**Table 1** Chemical composition of 2195-T8 Al-Li alloy.

| Cu | Li | Mg | Zr | Fe | Ag | Al |
|------|------|------|------|------|------|------|
| 3.99 | 1.09 | 0.38 | 0.11 | 0.17 | 0.42 | Bal. |

The tensile test specimens, with specific dimensions, see Figure 1, were prepared, from the welded plates. The loading direction on the tensile specimens was perpendicular to the welded line, based on standard GB/228.1-2010.
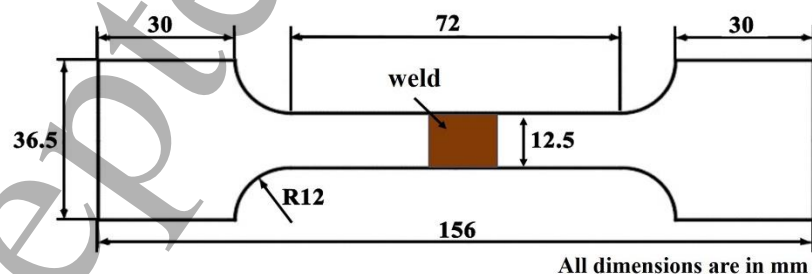


**Figure 1.** Dimensions of the test specimen.

Exfoliation corrosion (EXCO) was carried out based on standard ASTM G34 [40], using EXCO solution, which consists of 234 g NaCl + 50g $KNO_3$ + 6.3 mL $HNO_3$ / L. The standard ASTM G34 is suitable to be used for as received and welded specimen

and widely used to study exfoliation corrosion of Al alloy [35, 39, 40, 43]. This standard provides a prediction exfoliation corrosion behavior of alloys in various types of outdoor environments, especially in marine and industrial environments [40].

The ratio of the volume of the corrosive solution ($V_m$) to the exposed specimen surface area ($S_s$) is $V_m : S_s = 15$ mL/cm$^2$. After rinsing and drying, the specimens were placed in EXCO solution at $25 \pm 3$ °C. The welded specimens were exposed to exfoliation corrosion for 24, 48, 96, 192 and 384 hours. To enhance the reliability of results, each test was repeated three times. Moreover, the corrosive solution was replaced every 96 h to minimize the corrosion byproducts effects. Figure 2 shows a welded specimen, the gauge length completely immerses in the EXCO solution, one end fixed in the middle of the bottom surface of the container and another end vertically towards the top.
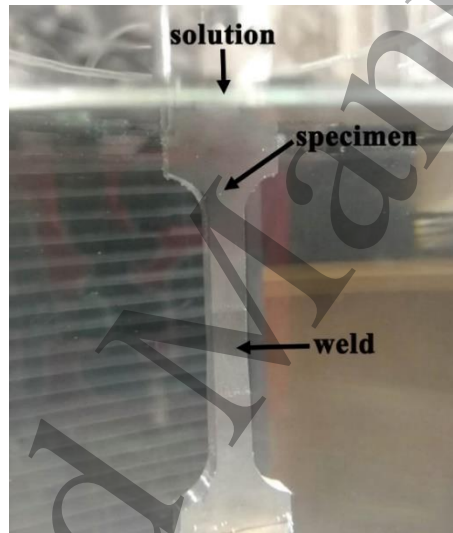


**Figure 2.** Schematic diagram of specimen placement.

The specimens were exposed to exfoliation tests, rinsed and dried. Then the samples were exposed to tension stresses using universal testing machine type WDJ-3008, the extension speed was 1 mm/min.

The corrosion morphology was observed by SU8020 scanning electron microscope (SEM). The microstructural changes of the joints of different welded zones were characterized by transmission electron microscopy (TEM), type FEI Tecnai G2 F20, operated at 200 kV. The specimens were prepared by twin-jet electro-polishing using a mixed solution of 30% $HNO_3$ + 70% $CH_3OH$ at -30°C, as it was carried out in the liquid nitrogen, which helps to control the polishing speed and preventing oxidation.

## 3. Results

### 3.1 Corrosion morphology

Figure 3 shows the corrosion morphology under SEM which would be helpful to investigate the EXCO corrosion process. Figure 3a shows the surface morphology of the unexposed to corrosion sample, where a large number of white precipitates were observed. Energy Dispersive Spectroscopy - EDS - results indicated as a point in the image associated with a graph, showed that the precipitation phase containing Al and Cu. Figure 3b shows that there are many corrosion pits after 24 h EXCO corrosion, which indicates that the corrosion phenomenon originates from pitting, even in EXCO tests in strong acid solutions. Tang *et al.* [47] and Ding *et al.* [48], reported that the corrosion of aluminum alloy in EXCO solution was mainly initiated by pitting, and finally developed into exfoliation corrosion. With time, the corrosion products accumulate continuously, as shown in Figure 3c and d. After removing the corrosion products by an external force, it was found, see Figure 3e, that the pits were expanding and forming connections. Figure 3f shows a surface morphology of the sample exposed to corrosion for 96 h, as a lot of "white filiform products" are shown and distributed at the bottom of the pits, caused by the continuous reaction of exposed new surfaces during the corrosion process [43]. Figure 3g and h, show more corrosion products accumulated on the surface after 192 h corrosion, showing a tendency of self-peeling. After removing the corrosion products, it was found that the corrosion was still ongoing under the corrosion pit covered by the corrosion products, and a large number of "white filiform product" corrosion products adhere to the bottom of the corrosion pits, see Figure 3i.
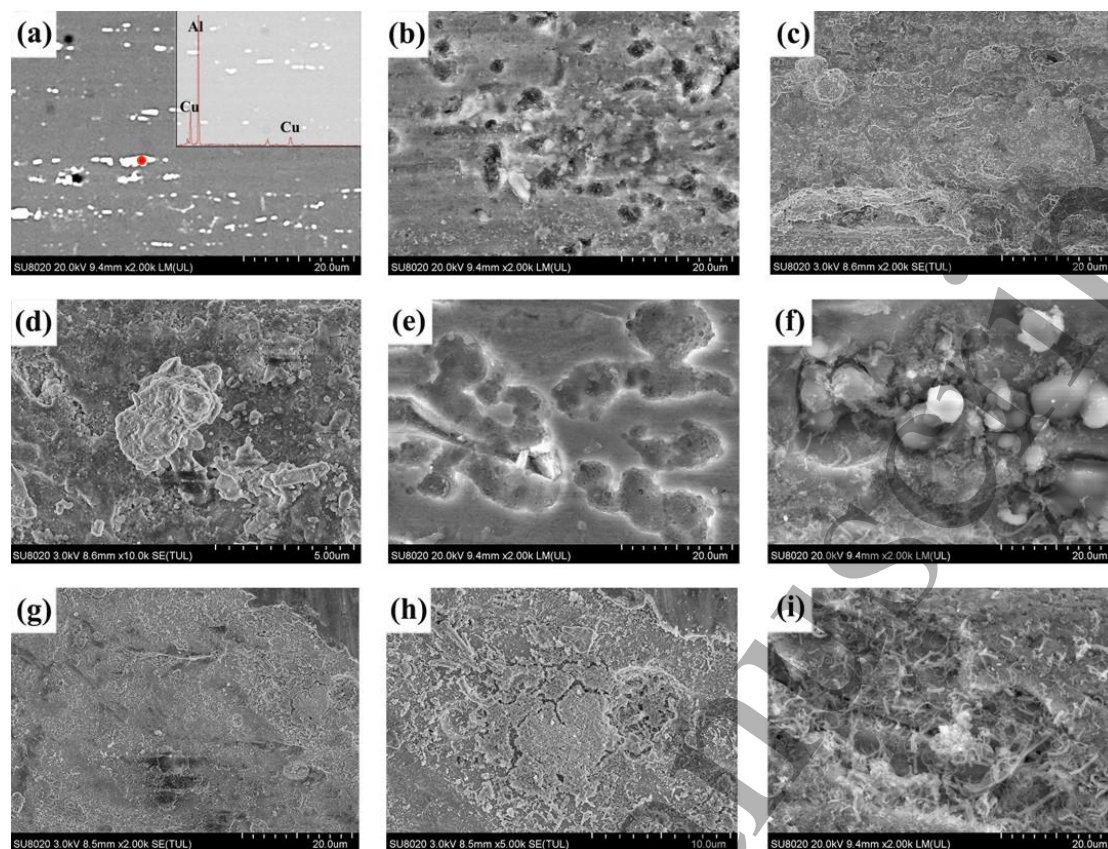
**Figure 3.** SEM morphology of the specimen (a) the material without corrosion, (b) corrosion 24 h, (c, d) corrosion products for 48 h, (e) pits after cleaning for 48 h corrosion, (f) corrosion for 96 h, (g, h) corrosion for 192 h, (i) pits bottom after corrosion 192 h.

## 3.2 Mechanical properties after corrosion

Figure 4 shows the stress-strain diagram of the friction stir welded specimens exposed to exfoliation corrosion for different times. The results showed that with increasing the exposure time, the mechanical properties gradually decreased. For example, with the exposure time equals 24 h, the ultimate tensile strength UTS was 430.9 MPa and the elongation 11.08%. With increasing the exposure time to 384 h, the UTS reduced to 386.7 MPa and the elongation to 9.31%.
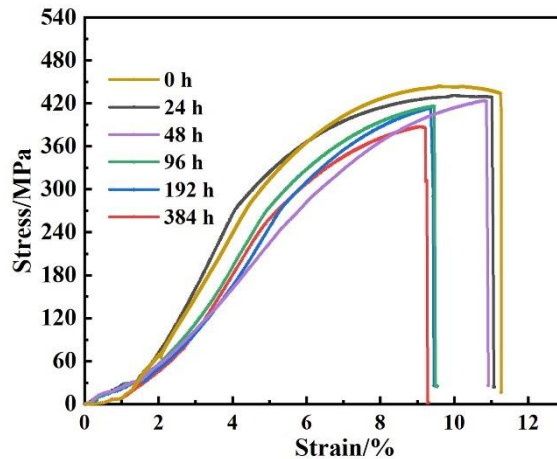
**Figure 4.** Stress-Strain diagram of Al-Li welded samples exposed to different corrosion times.

To identify the effect of the exposure time of the exfoliation corrosion on the mechanical properties of the welded specimens, the intensity ratio was calculated, which was defined as the ratio of the UTS of the tested specimens ($\sigma_{test}$) to the original, or unexposed to corrosion sample, UTS ($\sigma_o$), denoted as $\sigma_{test}/\sigma_o$. Thus, the strength loss rate $v_{sr}$ was defined as the rate at which the intensity ratio $\sigma_{test}/\sigma_o$ changed over time, t, using Equation (1):

$$v_{sr} = (1-\sigma_{test}/\sigma_o)/t \tag{1}$$

Similarly, the intensity ratio was calculated for elongation, as a ratio of elongation of the tested specimen (El$_{test}$) to the initial elongation (El$_o$), denoted as El$_{test}$/El$_o$. The elongation loss rate $v_{er}$ was defined as the rate at which the elongation ratio changed over time, using Equation (2):

$$v_{er} = (1-El_{test}/El_o)/t \tag{2}$$

Table 2 shows that both the tensile strength ($\sigma_o$) and the elongation (El$_o$) of the joint deteriorates of different exposure time.

**Table 2** Mechanical properties of the samples at different exposure times

| Times/h | $\sigma_{test}$/MPa | $El_{test}$/% | $\sigma_{test}/\sigma_o$ | $El_{test}/El_o$ | $v_{sr}$ ($\times10^{-3}$/h) | $v_{er}$ ($\times10^{-3}$/h) |
|---------|---------|---------|---------|---------|---------|---------|
| 0 | 443.7 | 11.27 | - | - | - | - |
| 24 | 430.9 | 11.08 | 97.1% | 98.3% | 1.21 | 7.08 |
| 48 | 423.4 | 10.91 | 95.4% | 96.8% | 0.96 | 6.67 |
| 96 | 416.3 | 9.55 | 93.8% | 84.7% | 0.65 | 1.59 |
| 192 | 413.4 | 9.42 | 93.2% | 83.6% | 0.35 | 0.85 |
| 384 | 386.7 | 9.31 | 87.2% | 82.6% | 0.33 | 0.45 |

Figure 5 shows the changes of the UTS and elongation with the corrosion exposure time. The figure has illustrated these changes in three stages. Figure 5a showed that the corrosion had the highest impact on the tensile strength of the joint at stage I ($t \leqslant 96$ h), the loss rate of the tensile strength equals 0.29 MPa/h. In stage II of corrosion ($96 < t \leqslant 192$ h), the loss rate equal to 0.03 MPa/h, which can be attributed to the formation of the corrosion products [46], were stuck to the surface of the joint and lowered the strength values. However, in stage III of corrosion ($192 < t \leqslant 384$ h), the tensile strength reduction rate was increased rapidly, and the loss rate was 0.14 MPa/h.
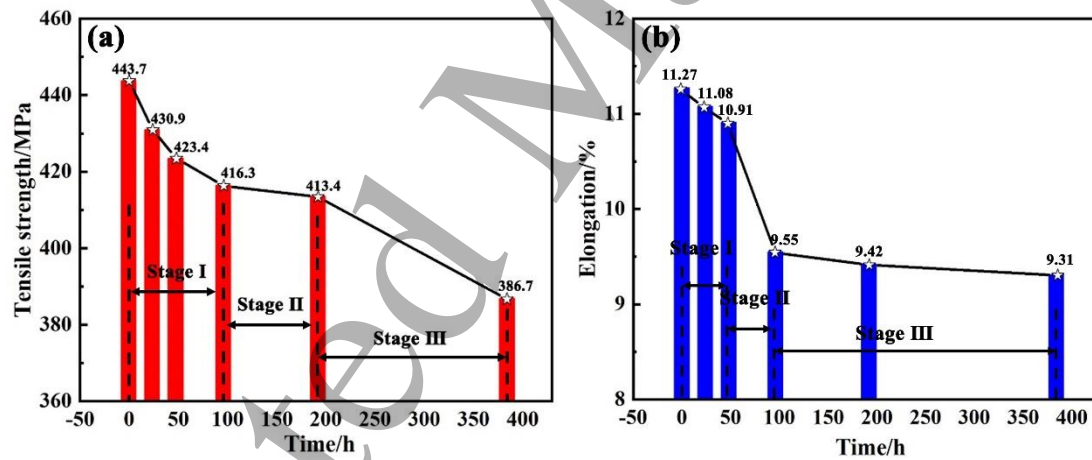


**Figure 5** Diagram shows the mechanical properties vs. the corrosion exposure time
(a) UTS-exposure time, (b) elongation-exposure time.

Figure 5b shows the influence of the corrosion exposure time on the elongation. The figure shows, similar to UTS, has divided into three stages, obviously with different rates. In stage I ($t \leqslant 48$ h), the joint ductility decreased with the occurrence of corrosion reaction, it was a slow process. In stage II of corrosion ($48 < t \leqslant 96$ h), the elongation decreased sharply and the slope of the curve in stage II was the highest, which means

that the elongation dropped sharply. In stage III ($96 < t \leqslant 384$ h), the elongation of the joint decreased slowly.

Figure 6 shows a diagram correlates between mechanical properties loss rate and corrosion exposure time of the joints. The highest UTS reduction rate was equal to $1.21 \times 10^{-3}$/h at an exposure time of 24 h, then gradually decreased for longer exposure times, the loss rate reduced to $0.33 \times 10^{-3}$/h for 384 h of corrosion. In terms of the elongation loss rate, the value dropped sharply in the latter part of the early stage of corrosion. In the interval from 48 h to 96 h, the elongation loss rate dropped from $6.67 \times 10^{-3}$/h to $1.59 \times 10^{-3}$/h, with a decrease of 319%.
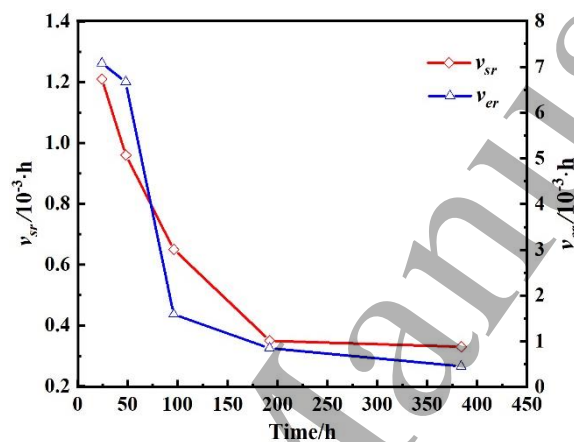


**Figure 6.** Intensity ratio change vs. the exposure time of welded samples.

### 3.3 Empirical equation

The results in Table 2, UTS and elongation vs. exposure time, were integrated - using MATLAB - to establish equations 3 and 4, which expect the effect of the exposure corrosion time on UTS and El% respectively. The fitting results as shown in Table 3.

$$\sigma_t = -4.186 \times 10^{-6} t^3 + 0.0028 t^2 - 0.515 t + \sigma_o \qquad (3)$$

$$El_t = -7.426 \times 10^{-10} t^3 + 7.169 \times 10^{-7} t^2 - 0.00022 t + El_o \qquad (4)$$

**Table 3** Fitting results of the mechanical properties of the joints.

|                  | σ-Exposure time | El-Exposure time |
| ---------------- | --------------- | ---------------- |
| SSE              | 3.279           | 3.972            |
| $R^2$            | 0.9979          | 0.9224           |
| Confidence level | 95%             | 95%              |

Sum of Squared Errors - SSE value could judge the degree of data fitting, the smaller of SSE, the better of fitting degree. In statistics, $R^2$ is the determining coefficient ranges between 0 and 1. Based on the fitting equation of σ-Exposure time - assuming

the joint failed when the strength of the joint reaches a specific value after corrosion - the service life of the joint in a solution similar to EXCO solution can be estimated. When $R^2$ is equal to or close to 1, it indicates that the fitting results are relatively accurate. Based on Table 3, the SSE and $R^2$ in the fitting results of the σ-Exposure time were 3.279 and 0.9979, while in the fitting results of El-Exposure time were 3.972 and 0.9224, which means that the fitting degree of σ-Exposure time was more sufficient. The fitting results of $R^2$ in the Equation (3) and (4) were both close to 1, and the confidence level was both 95%, indicating that the regression fitting result was satisfied.

The Equation (3) and (4) were combined to cubic functions and could be expressed as Equation (5):

$$f(\text{property}) = at^3 + bt^2 + ct + d \tag{5}$$

were a, b and c are the coefficients related to the equation, and d was a constant of the equation.

Equation 5 can be used to calculate the effect of the exfoliation corrosion time on the mechanical properties of welded FSW Al-Li alloy type 2195-T8.

### 3.4 Microstructural Evolution of the Weldments

Figure 7a, b and c show the TEM images of the base metal. The figures show that there are laminar-like $T_1$ phases arranged in a specific direction in the BM sample, which has been indicated by other researchers [11, 14, 15]. In addition to the $T_1$ phase, some θ′ phase was observed. However, $T_1$ phase, with high electrochemical activity, precipitates preferentially at grain boundaries, sub-grain boundaries and dislocations, are the main places of corrosion selectivity [22, 29].
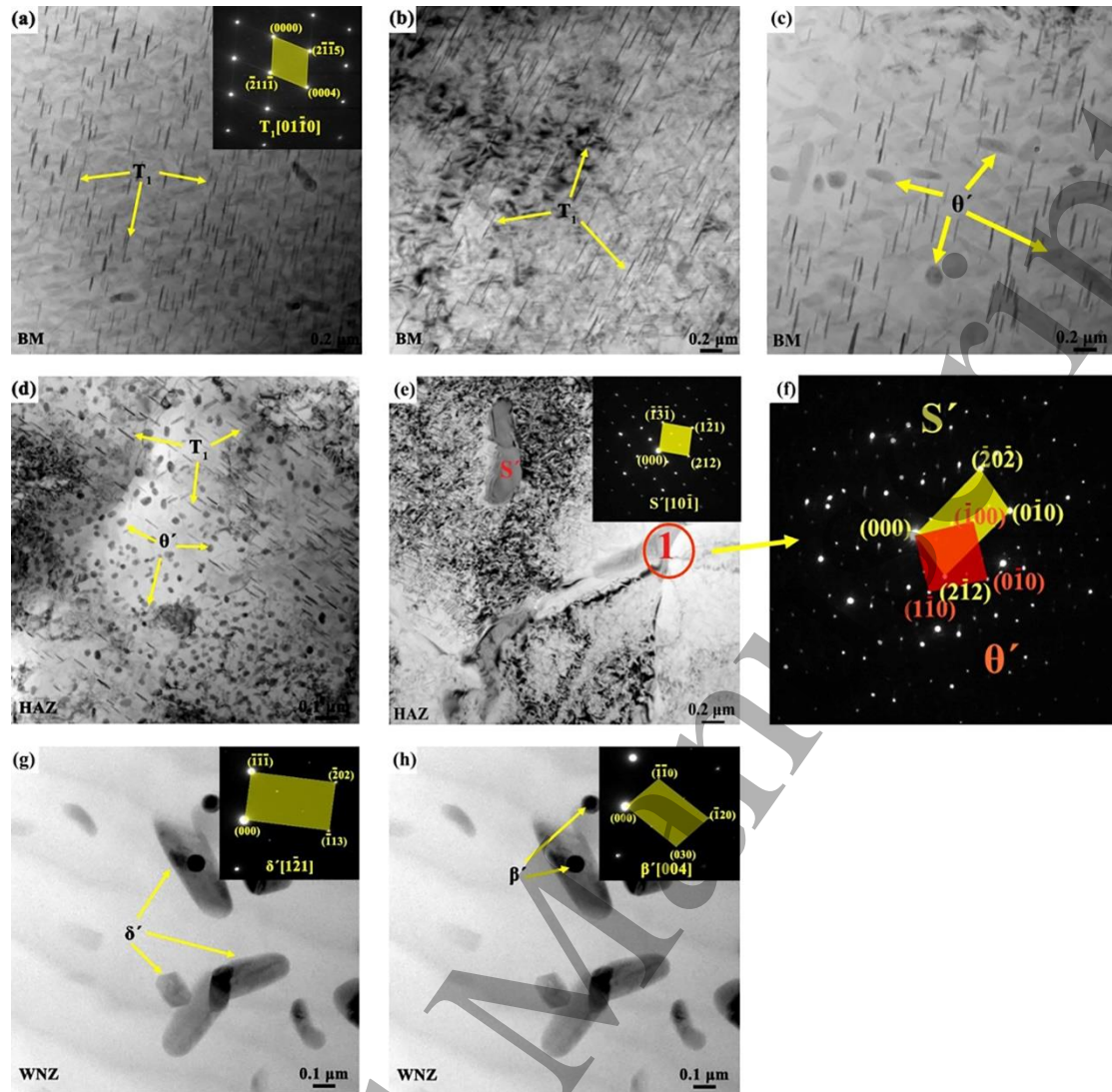
**Figure 7.** TEM images and the associated SAD patterns of friction stir welded 2195-T8 alloy joint: (a and b) BM, (c and d) HAZ, and (e and f) WNZ.

Figures 7d, e and f show the TEM images of the HAZ. A large number of $\theta'$ and $T_1$ precipitates can be seen in Figures 7d and e. This is an indication that during the welding process, parts of $T_1$ precipitates have dissolved and accumulated, while growth of $\theta'$ precipitates occurs in specific regions within HAZ. Besides, the $S'(Al_2CuMg)$ phase was observed in HAZ, see Figure 7e, which can be attributed to the $S'$ has precipitated under the action of heating during welding. The $S'$ phase, as a vulnerable phase [20, 21], acts as anode and preferential corrosion. Both $\theta'$ and $S'$ phases can be observed in intergranular precipitates, see Figures 7e and f, which lead to a further reduction in the corrosion resistance of HAZ.

Figures 7g and h show the TEM images of WNZ region. The precipitated $T_1$ and $\theta'$ phase were transformed into the $\delta'$ phase and $\beta'$ ($Al_3Zr$) phase.

## 4. Discussion

Aluminum, magnesium and lithium are sensitive to highly acidic solutions due to their high electrochemical activity [22, 46], they all have negative electrochemical force values, which is also called corrosion potential [31]. Hydrogen ions in the acidic environment (EXCO solution) receive electrons consequently hydrogen released, which acts as a driving force for corrosion occurrence.

Figure 4 showed the mechanical properties of the welded Al-Li alloy were negatively interrelated with the exposure time. This could be attributed to the fact that since corrosion induces surface pits with time while it is in contact with a corrosive solution, and it has a profound effect on property degradation of materials, thus the longer the exposure time, the lowest the mechanical properties of the joint [39, 44]. Similarly, the elongation decreased with the increase of corrosion time, which was related to a transverse pit/crack defect caused by the applied stress and the decrease of the cross-sectional area of samples. These results are similar to other researches, Qiu [39], Nikolaos *et al.* [49] and Leslie *et al.* [50], reported that such degradation process was mainly due to the reaction between the solution and the surface areas where the phases, $T_1$ and $S´$ phase, have existed, which are acting to reduce the effective cross-sectional area, i.e. coherency, and the surface pits caused by corrosion would induce the formation of transverse cracks, consequently, the degradation occurs.

Figure 5 showed the changes of the UTS and elongation with the corrosion exposure time. The figure showed that both mechanical properties, UTS and elongation, were divided into three stages. In correlation with the microstructure analysis in Figure 7 and based on other researches studied the influence of microstructure on the corrosion behavior of Al-Li alloy [17-21], the three stages behavior could be explained in a way that, $T_1$ and $S´$ were consumed continuously due to the priority of corrosion during the corrosion process [14, 15], the continuous corrosion leads to a reduction in UTS values, see Figure 5a. While the tensile strength of the joints becomes lower due to the corrosion phenomenon of the preferential phases, the corrosion byproducts generate, gathered, adhered to the surfaces, thus the early elastic drop appears. The protection of corrosion products for the decline of elongation in the middle stage of corrosion makes stage III of elongation decline tend to be steady.

The three stages in Figure 5a of the influence of corrosion on the tensile strength of the joint could be summarized as the following three steps:

In stage I ($t \leqslant 96$ h), while the corrosive solution is in contact with the substrate, corrosion reaction occurs, it first reacted with the corrosive phases, such as $T_1$ and $S'$ [16, 17] and this affected the tensile strength of the joint, thus the UTS decreased significantly.

In stage II ($96 < t \leqslant 192$ h) the reduction rate of UTS was slowed down, which was related to the formation of corrosion products, adhere to surfaces, thus the contact between the corrosive environment and the substrate become limited. Similar approaches have been mentioned by other researchers, Su *et al.* [46], Sun *et al.* [51] and João *et al.* [52] the protective effect of corrosion products on the matrix was reported, the existence of this isolation effect would slow down the corrosion reaction, thus reducing the degradation rate.

In stage III ($192 < t \leqslant 384$ h), after a long exposure time, a large amount of corrosion products has been generated and accumulated, but because the amount of insoluble corrosion products was larger than the amount of the corroded metal, this was resulting in "wedge effect" [20, 47, 48], see Figure 3g and h, which supported by the uncorroded metal in the upper layer and caused layer peeling [39, 49], the decreased of the effective cross-sectional area made the tensile strength decline rapidly.

For the changes in elongation, shown in Figure 5b, although it was also divided into three stages, the reduction rates were different than the UTS. This is because the increase of joint ductility by corrosion was mainly related to the corrosion consumption $T_1$ and $S'$, and the generation, adhesion, and shedding of corrosion products also played a certain role in the change of joint.

In stage I ($t \leqslant 48$ h), the $T_1$ phase was corroded first and the pits were small, therefore the elongation does not decline very quickly. However, when the corrosion continues to stage II ($48 < t \leqslant 96$ h), a large amount of $T_1$, surrounded by aluminum matrix were dissolved, then exposed $S'$ phase begins to corrode, and the corrosion holes were interconnected and aggregated to form bigger weak areas. The common influence of the $T_1$ and $S'$ phases, and the formation of weak areas [39], so the elongation decreases rapidly. In the stage III ($96 < t \leqslant 384$ h), a large number of corrosion products were generated and adhered, filled up some gaps and pits on the surface, which compensated the loss of the cross-sectional area due to previous stages of corrosion [39], leading to a reduction in the rate of the change. Even after the spalling of the specimen, the cross-sectional area decreased, and the new surface was exposed, but the

presence of many uncorroded and strengthened phases $T_1$, see Figure 7, caused a decline of elongation not significant.

Figure 7 showed $\theta'$ phase as the main strengthening phase of Al-Li alloy. Because Cu has a high electrochemical force which makes this phase acts as cathode compared to Al substrate and the $T_1$ phase, leading to the dissolution of the surface of the Al alloy [20, 30]. Moreover, S´ phase is prone to corrosion, its quantity was far less than that of $T_1$ phase, and its corrosion resistance was slightly higher than that of $T_1$ phase [31]. These are the reasons behind the fact that the reduction of strength and elongation in the corrosion process was not completely linear. On the other hand, both $\delta'$ and $\beta'$ phases have low electrochemical activity, i.e. high corrosion potential, but they were both the strengthening phases of Al-Li alloy [23, 34]. Therefore, during the corrosion process, the joint performance did not show a completely linear relationship with the corrosion, see Figure 6, due to the consumption of $T_1$ and S´.

## 5. Conclusions

- Exfoliation corrosion acted to reduce the UTS and El% of FSW Al-Li type 2195-T8. The UTS values were decreased at different rates with the corrosion exposure times, 97% within 24 h, 95% in 48 h, 94% for 96 h, 93% for 192 h and 87% in 384 h, compared with the initial UTS equals to 443.7 MPa. While, for the same exposure times, El% was reduced by 98%, 97%, 85%, 84% and 83% comparing with the initial El, was equal to 11.27%.

- The degradation rate of the exfoliation corrosion on the mechanical properties was divided into three stages: for UTS, fast (0-96 h - the degradation rate was 0.29 MPa/h), steady (96-192 h - the rate equals 0.03 MPa/h) and medium (192-384 h - the rate was 0.14 MPa/h). While for El%, the rate was divided into slow (0-48 h - the degraded rate was 0.008%/h), fast (48-96 h - the rate was 0.028%/h) and steady (96-384 h - the rate was 0.001%/h).

- The degradation of welded specimens due to the exfoliation corrosion was interrelated with the microstructure, mainly to the dissolution of $T_1$ phase and S´, generation corrosion byproducts, adhesion with the surfaces and shedding the surfaces affected the change of the joint performance, mainly in stage II and stage III.

- A mathematical equation has been derived to predict the effect of the exfoliation corrosion exposure time on the mechanical properties of the FS welded Al-Li alloy type 2195-T8.

## Acknowledgments

## References

[1] El-Aty A A, Xu Y and Guo X-Z 2018 Strengthening mechanisms, deformation behavior, and anisotropic mechanical properties of Al-Li alloys, A review Journal of Advanced Research 10 49-67.

[2] Tolga D and Costas S 2014 Recent developments in advanced aircraft aluminum alloys Materials & design 56 862-71.

[3] Yuan T, Jiang J-H and Wang L-S 2019 Overview on the microstructure and mechanical properties of ultrafine-grained Al-Li alloys produced by severe plastic deformation, Rare Metal Materials and Engineering 48 0055-62.

[4] Sun Y-M 2018 A study on high performance Al-Li casting alloys Shenyang Aerospace University 1-58.

[5] Wu X-L, Liu M and Zang J-X 2016 Research progress and aerospace applications of aluminum-Lithium alloys Materials Reviews 30 571-8+585.

[6] Wang G-Q and Zhao Y-H 2010 Friction stir welding of aluminum alloy. China aerospace publishing house, China.

[7] Ma Z-Y, Feng A-H and Chen D-L 2018 Recent advances in friction stir welding/processing of aluminum alloys, microstructural evolution and mechanical properties Critical Reviews in Solid State and Material Sciences 43 269-333.

[8] Mishra R S and Ma Z-Y 2005 Friction stir welding and processing Materials Science and Engineering: R 50 1-78.

[9] Qin H-L 2014 The study of microstructures and mechanical properties of Friction Stir Welded and YAG-MIG hybrid welded joints for 2195 alloy University of Science and Technology Beijing.

[10] Song J-L, Wang L and Zhao Y-J 2019 Friction stir welding process of 2195 Al-Li alloy Weld 31-5+66.

[11] Nayana N, Yadava M, Sarkar R, Narayana Murty S V S, Gurao N P, Mahesh S, Prasad M J N V and Samajdar I 2020 Microstructure and tensile response of friction stir welded Al-Cu-Li (AA2198-T8) alloy Materials Characterization 159 110002.

[12] Zhao C-Y, Yang R-S, Zhang H, Guo Q-L, Shao T-G, Liu G-R 2020 Structure and corrosion resistance of cold spray coating prepared on friction stir welded high strength aluminum alloys Journal of Aeronautical Materials 40 28-34.

[13] Sunil S and Kumar D D 2020 An experimental investigation to the influence of traverse speed on microstructure and mechanical properties of friction stir welded AA2050-T84 Al-Cu-Li alloy plates Journal of Materials Processing Technology 277 116482.

[14] Qin H-L, Zhang H and Wu H-Q 2015 The evolution of precipitation and microstructure in friction stir welded 2195-T8 Al-Li alloy Materials Science and Engineering: A 626 322-9.

[15] Cai C, Li Y, Li J-F, Zhang Z and Zhang J-Q 2019 Correlation Between Ageing Precipitation, Potential and Intergranular Corrosion of 2A97 Al-Li Alloy Sheet Acta Metallurgica Sinica 55 958-66.

[16] Meng Q, Liu Y, Kang J, Fu R-D, Guo X-Y and Li Y-J 2019 Effect of precipitate evolution on corrosion behavior of friction stir welded joints of AA2060-T8 alloy Transactions of Nonferrous Metals Society of China 29 701-9.

[17] Sidhar H, Y. Martinez N, S. Mishra R and Silvanus J 2016 Friction stir welding of Al-Mg-Li 1424 alloy Materials & Design 106 146-52.

[18] Entringer J, Meisnar M, Reimann M, Blawert C, Zheludkevich M and F. dos Santos J 2019 The effect of grain boundary precipitates on stress corrosion cracking in a bobbin tool friction stir welded Al-Cu-Li alloy Materials Letters: X 2 100014.

[19] Entringer J, Reimann M, Norman A and F. dos Santos J 2019 Influence of Cu/Li ratio on the microstructure evolution of bobbin-tool friction stir welded Al-Cu-Li alloys Journal of Materials Research and Technology 8 2031-40.

[20] Ren W-D, Li J-F and Zheng Z-Q 2007 Localized corrosion mechanism associated with precipitates containing Mg in Al alloys Transactions of Nonferrous Metals Society of China 17 727-32.

[21] Bousquet E, Poulon-Quintin A, Puiggali M, Devos O and Touzet M 2011 Relationship between microstructure, microhardness and corrosion sensitivity of an AA 2024-T3 friction stir welded joint Corrosion Science 53 3026-34.

[22] Zolghadr P, Akbari M and Asadi P 2019 Formation of thermo-mechanically affected zone in friction stir welding Materials Research Express 6 086558.

[23] X. Milagre M, V. Mogili N, Donatus U, A.R.Giorjão R, Terada M, S. Araujo J V, S.C. Machado C, Costa I 2018 On the microstructure characterization of the AA2098-T351 alloy welded by FSW Materials Characterization 140 233-46.

[24] Gao C, Zhu Z-X, Han J and Li H-J 2015 Correlation of microstructure and mechanical properties in friction stir welded 2198-T8 Al-Li alloy Materials Science & Engineering A 639 489-99.

[25] Liu D-Y, Li J-F, Lin Y-C, Ma P-C, Chen Y-L, Zhang X-H and Zhang R-F 2020 Cu/Li Ratio on the Microstructure Evolution and Corrosion Behaviors of Al–xCu–yLi–Mg Alloys Acta Metallurgica Sinica (English Letters) xx xx-xx(Online).

[26] X. Milagre M, Donatus U, V. Mogili N, P. Silva R M, G. de Viveiros B V, F. Pereira V, A. Antunes R, S.C. Machado C, S. Araujo J V and Costa I 2020 Galvanic and asymmetry effects on the local electrochemical behavior of the 2098-T351 alloy welded by friction stir welding Journal of Materials Science & Technology 45 162-75.

[27] Liu D-Y, Sang F-J, Li J-F, Birbilis N, Wang Z-X, Ma Y-L and Zhang R-F 2019 The role of grain structure

characteristics on the localised corrosion feature in the 1445 Al-Cu-Li alloy Materials Characterization 158 109981.

[28] Zheng Y-Y, Luo B-H, He C and Su Y-L 2019 Effect of aging time on microstructure evolution and corrosion behavior of an Al-Mg-Si alloy Materials Research Express 6 116582.

[29] Ma Y-L, Meng X-M, Huang W-J and Zhang X-B 2015 Effect of microstructural heterogeneity on localized corrosion of AA2099-T8 aluminum-lithium alloy The Chinese Journal of Nonferrous Metals 25 611-7.

[30] Chen X-R, Zheng Z-Q, Ye Z-H and Kong X 2018 Microstructure characterization of friction stir welded 2099 Al-Li alloy Rare Met Mater Eng. 47 1786-92.

[31] Yi J-L, Chen L and Chen J 2011 Function mechanism of main secondary phases generated by alloying on localized corrosion of Al-Li alloy Corrosion & Protection 32 822-5+844.

[32] Xu R-Z, Wei Z-C and Guo X M 2017 Review of Studies on Friction Stir Welding for Aluminum-Lithium Alloy Materials Reviews 31 323-6.

[33] Chu Q, Li W-Y and Yang X-W 2018 Microstructure and mechanical optimization of probeless friction stir spot welded joint of an Al-Li alloy Journal of Materials Science & Technology 34 1739-46.

[34] Zhang J, Feng X-S and Gao J-S 2018 Effects of welding parameters and post-heat treatment on mechanical properties of friction stir welded AA2195-T8 Al-Li alloy Journal of Materials Science & Technology 34, 219-27.

[35] Li J-F, Zheng Z-Q and Li S-C 2004 Study on intergranular corrosion and exfoliation corrosion behaviors of 2195 Al-Li alloy Journal of Materials Science and Engineering 22 640-3.

[36] Huang J-L, Li J-F and Liu D-Y 2018 Correlation of intergranular corrosion behaviour with microstructure in Al-Cu-Li alloy Corrosion Science 139 215-26.

[37] Luo C, Sergiu P A and Zhou X R 2016 Continuous and discontinuous localized corrosion of a 2xxx aluminum-copper-lithium alloy in sodium chloride solution, Journal of Alloys and Compounds 658, 61-70.

[38] Li J-F, Chen W-J and Zhao X-S 2006 Corrosion behavior of 2195 and 1420 A1-Li alloys in neutral 3.5% NaCl solution under tensile stress Transactions of Nonferrous Metals Society of China 16, 1171-7.

[39] Qiu T, Tang X-W and Song J-H 2018 Quantitative relation between corrosion damage and mechanical parameters of 2024-T4 aluminum alloy Nonferrous Metals Engineering 8 19-24.

[40] ASTM G34 (Reapproved 2013). Standard Test Method for Exfoliation Corrosion Susceptibility in 2XXX and 7XXX Series Aluminum Alloys (EXCO Test).

[41] Liao W-B, Liu X-Y and Liu S D 2012 Effect of exfoliation corrosion on mechanical properties of 7055 aluminum alloy sheet Journal of Central South University (Science and Technology) 43 2137-41.

[42] Wang J 2010 Study of 7075 alloy atmospheric corrosion test in the marine environment Shenyang Aerospace University 1-57.

[43] Khoshnaw F M and Gardi R H 2007 Effect of aging time and temperature on exfoliation corrosion of aluminum alloys 2024-T3and 7075-T6 Materials & Corrosion 58 345-7.

[44] Ma S-H, Fei B-Q and Zhou S 2017 Influence of pre-corrosion damage and saline environment on detail fatigue property of aluminum alloy Materials for Mechanical Engineering 41 63-7+73.

[45] Lu Q-B, Long W-M and Shen Y-X 2016 The corrosion resistance and mechanical properties of welding joint

of 5083 aluminum alloy Welding Digest of Machinery Manufacturing 9-11.

[46] Su Y, Zhang L-W and Zhong Y 2016 Marine atmospheric corrosion behavior of 5A90 Al-Li Alloy Journal of Chinese Society for Corrosion and Protection 36 260-6.

[47] Tang Z-Q, Jang F, Long M-J, Jiang J-Y, Liu H-F and Tong M-M 2020 Effect of annealing temperature on microstructure, mechanical properties and corrosion behavior of Al-Mg-Mn-Sc-Zr alloy Applied Surface Science 514 146081.

[48] Ding Q-W, Zhang D, Yan Y, Zhuang L-Z and Zhang J-S 2020 Role of subgrain stripe on the exfoliation corrosion of Al-4.6Mg-3.1Zn (wt.%) alloy Corrosion Science 169 108622.

[49] D. Alexopoulos N, Proiou A, Dietzel W, Blawert C, Heitmann V, Zheludkevich M and K. Kourkoulis S 2016 Mechanical properties degradation of (Al-Cu-Li) 2198 alloy due to corrosion exposure Procedia Structural Integrity 2 597-603.

[50] G. Bland L, Zhu Y-K, Pope J, Mills L, Garofano J, Smith K and Locke J 2018 Comparison of Corrosion Performance of AA7075 and AA2070 in Various Test Environments Corrosion 75 549-63.

[51] Sun S-Q, Zheng Q-F, Li C-L, Wang X-M and Hu S-Q 2017 Effect of Corrosion Products on Long-term Atmospheric Corrosion of Pure Aluminum 8A06 Journal of Chinese Society for Corrosion and Protection 37 110-6.

[52] Victor de Sousa Araujo J, Donatus U, Queiroz F M, Terada M, Milagre M X, Cavalieri de Alencar M and Costa I 2018 On the severe localized corrosion susceptibility of the AA2198-T851 alloy Corrosion Science 133 132-40.